UNIVERSITY OF COPENHAGEN
FACULTY OF SCIENCE

M.Sc. thesis

High-energy neutrino emission from supernovae

Submitted by : *Amit Singh*

Supervised by : *Dr. Irene Tamborra*

Date of Submission : May 22, 2023

Acknowledgements

Firstly, I would like to thank my supervisor Dr. Irene Tamborra, who was always there to guide me and correct me on my mistakes. Her patience and support when I was lazy or things were not going as planned, never made me lose my confidence. I really appreciate her supervision which made me learn and do most of the things on my own.

I would also like to extend my heartfelt gratitude to Tetyana Pitik and Ersilia Guarini for giving their valuable time throughout the thesis, for the many insightful discussions, and for the unyielding enthusiasm they vested in my doubts and problems. I am also thankful to all the other fellows of the AstroNu group for maintaining a good social and research environment, I learned many new things from their varied research works and weekly group meetings. It proved to be an opportunity for a great academic experience for me.

Last but not least, I would like to thank my parents and my brother for their constant moral support. Their words are the only thing that kept me going through the bleakest of times. Their love and confidence in me, nurtured my passion for pursuing research in Astrophysics, for which I will forever be grateful.

Abstract

Neutrinos with energies above a few TeV are produced in supernovae as a result of proton-proton interactions as the shock propagates in the circumstellar medium. In addition, neutrinos of high energy can be produced if a jet is harbored and choked in the supernova envelope. In this scenario no electromagnetic radiation would be visible. In this project, we will explore these different explosion scenarios and explore how to discriminate the explosion mechanism through non-thermal neutrinos.

The models described lead to TeV neutrino production through different non-thermal particle cooling methods like proton-proton collision, photo-proton collision, synchrotron, Inverse Compton, and the Bethe-Heitler process. These processes decide the cooling timescale which then compared to the acceleration timescale due to the magnetic field gives the maximum energy the hadrons and leptons can accelerate to. We aim to extend the detection horizon of Ice-Cube by proposing expected neutrino spectra and event rates from these mechanisms and discuss how good the predictions and the detections could be, for an event in Milky Way.

Contents

List of Figures

Chapter 1

Introduction

Before studying the neutrino emission from the supernovae, it's very important to know the physics behind the supernova explosions, the very basics of which are driven by the properties of progenitor stars. After this, we will shed some light on the abundant "ghost particles" of the universe referred to as Neutrinos. It is one of the many particles produced in supernova explosions and has proved to be very promising as a probe of the universe.

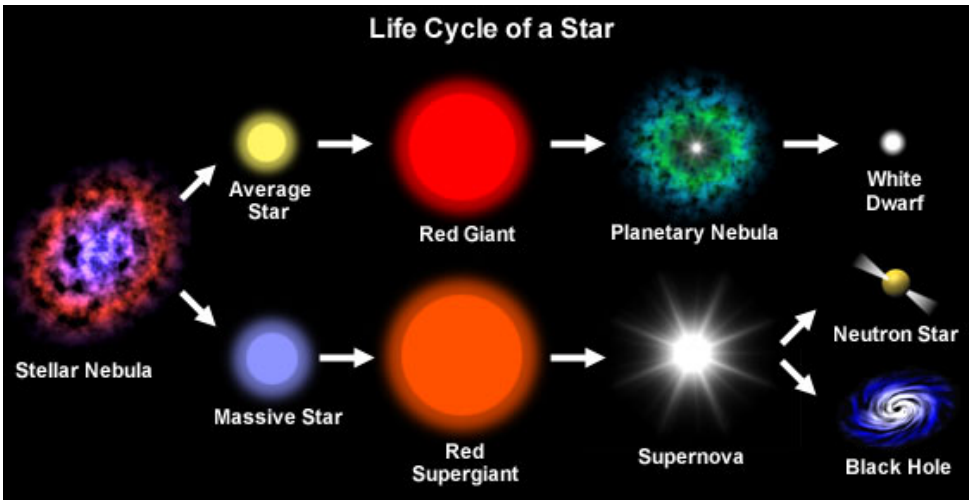

Figure 1.1: Life cycle of star
Credits : NASA

1.1 Supernovae

When a massive star ($>8M_{\odot}$ approx.) reaches the end of its evolutionary cycle and collapses under its own gravity or a binary star system with a white dwarf is triggered into a runaway fusion reaction, these conditions lead to a violent expulsion of outer layers of the star referred to as supernova. Supernova explosions(SNe) have a short observation time window but have a high peak optical luminosity before fading away, this increases the need for their exploration as they can give more information in less time [1].

Supernovae are a site of extreme particle acceleration and sources of various particles in our universe, one of them being neutrinos. They are also considered one of the sources of elements heavier than iron through neutron capture by atomic nuclei. These atomic nuclei are formed by nucleosynthesis when nuclear fusion takes place at a collapse-induced shockwave in the stellar envelope. Therefore, one can say that such cosmic explosions are essential for the biological life forms consisting of these heavy elements like iron, zinc, manganese, etc. [2]

Some of the bright SN in our Milky Way galaxy have been directly observed by people back in history. The rate of SNe in the Milky Way is about three stars per century making it important to look outside the Milky Way [1]. Fortunately, transient astronomy is growing rapidly and hundreds of such transient events are being observed every night with the help of various wide-field sky surveys like the Palomar Transient Factory (PTF), Zwicky Transient Facility (ZTF), upcoming Large Synoptic Survey Telescope (LSST), etc.

1.1.1 Classification

Supernovae are classified on the basis of their spectral features and sometimes by the light curves. They are broadly classified into two categories type-I and type-II depending on the presence of hydrogen lines in the spectrum. Type-I is further subcategorized into three groups on the basis of the silicon absorption feature and the presence of helium lines in the spectrum whereas type-II is subcategorized into

four types depending upon the shape of the light curve and the spectrum [3][4] as shown in Table 1.1.

Supernova taxonomy

<table>
<tr><td rowspan="2">Type I
no hydrogen</td><td colspan="2">Type Ia
presence of Si line</td><td>Thermonuclear</td></tr>
<tr><td rowspan="2">Type Ib/c
no Si absorption feature</td><td>Type Ib
shows a He line</td><td rowspan="5">Core-collapse</td></tr>
<tr><td>Type Ic
weak or no He line</td></tr>
<tr><td rowspan="4">Type II
shows hydrogen lines</td><td colspan="2">Type II-P
reaches a ”plateau” in its light curve</td></tr>
<tr><td colspan="2">Type II-L
displays a ”linear” mag. decrease in light curve</td></tr>
<tr><td colspan="2">Type IIn
narrow spectral lines</td></tr>
<tr><td colspan="2">Type IIb
broad spectral lines</td></tr>
</table>

Table 1.1: Supernovae classification and process driving them [3][4].

Further in Fig 1.2, we can see the typical light curves for different supernovae. These light curves don't insist on any specific values for a given type but compare a general trend of how they look for different supernovae types. We can see the light curve of supernova II-P is flat between day-10 and day-90 whereas for II-L it is decreasing linearly till the end. SN Ia is generally the brightest of all emitting $\geq 10^{43}\ erg/s$ in optical, billion times that of the Sun and is driven by the runaway thermonuclear mechanism whereas the rest of them are driven by the core-collapse mechanism. However, core-collapse supernovae are more energetic than Ia. A few percent of the type Ib/c supernovae are associated with gamma-ray bursts (GRB) as well. Let's keep in mind, light curves of Ib-Ic or IIb-IIn may or may not be alike because their classification is based on absorption spectral features rather than light curves.

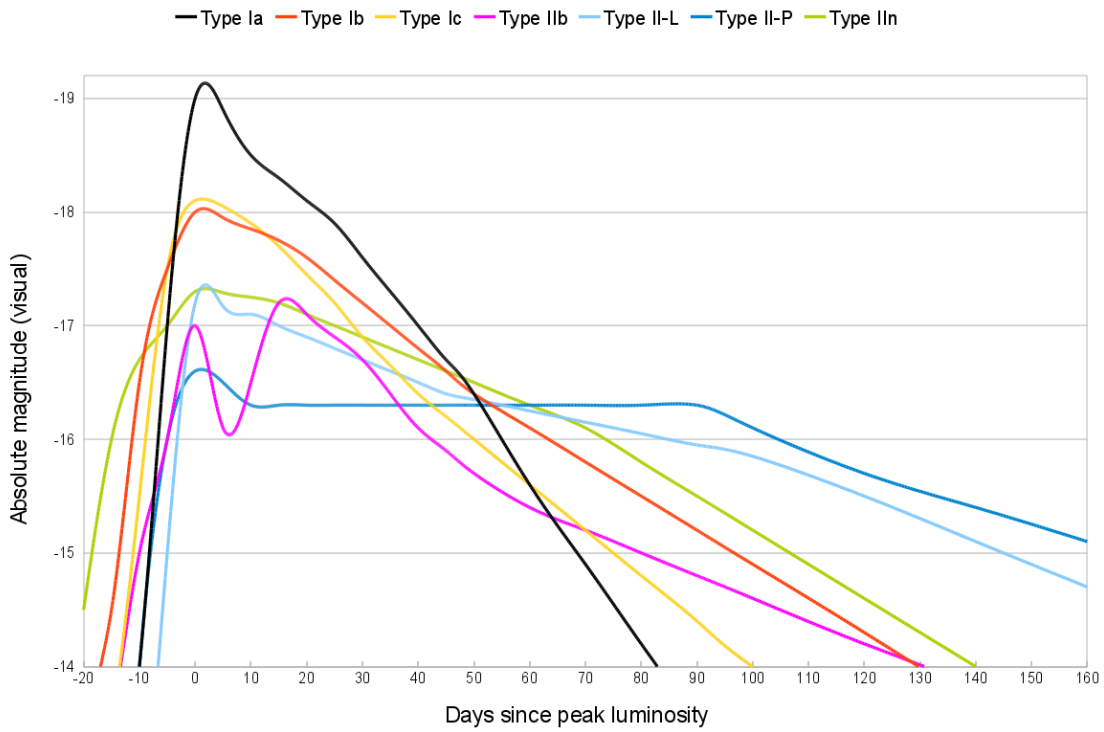

Figure 1.2: Typical light curves for several types of supernovae; in practice, magnitude, and duration varies within each type. See [5] for types Ia, Ib, II-L and II-P; [6] for types Ic and IIb; and [7] for type IIn.

Well, the classification has always been on how the supernova looks and what are its properties but not necessarily on its cause. Supernovae are driven by either runaway thermonuclear or core-collapse mechanisms. Let's talk a little about the mechanism driving them.

1.1.2 Runaway thermonuclear supernova

A runaway thermonuclear SN happens in a binary system consisting of a white dwarf accumulating material from a close companion star. This increase in mass at a high accretion rate increases the core density and temperature enough to ignite the fusion, which results in a runaway thermonuclear reaction, completely destroying it. The fusion reactions continue all the way up until iron group elements are produced throughout the star. There are two theoretical ways: accretion of material from a companion star probably a giant or the collision of two white dwarfs. The dominant

mechanism by which type Ia supernovae are produced remains unclear [8].

SN Ia has very uniform properties and is useful standard cosmic candles over intergalactic distances, even if there is no surety about the underlying mechanisms. Some calibrations are required to compensate for small variations in brightness or for the gradual change in properties of abnormal luminosity supernovae [9][10] (in which the mass exceeds Chandrashekhar limit [11] but have less ejected kinetic energy than normal and is supported by the rotation of star [12]).

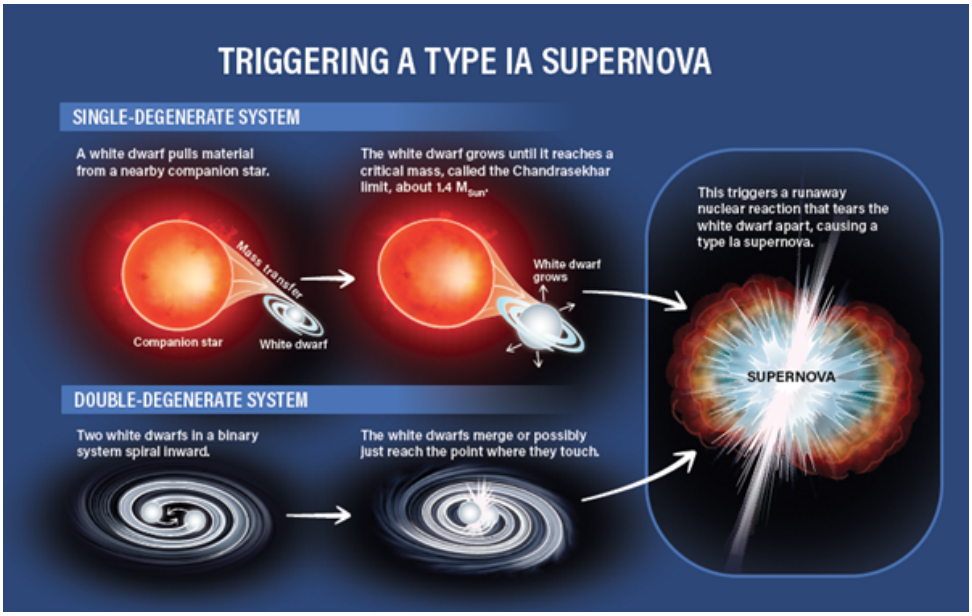

Figure 1.3: Runaway thermonuclear mechanism for SN Ia. [13]

1.1.3 Core-collapse SN

A core-collapse supernova can be either type I (Ib/c) or type II (II-P/L/n/b), as discussed in 1.1.1 the only observational distinction between them is the presence or absence of hydrogen lines in their spectrum.

When a massive star is exhausted of hydrogen for burning, the core pressure drops and it can't sustain against its own gravity. As a result, the core is compressed and simultaneously heated up initiating further fusion reaction. While the core contracts and produce elements till iron through nuclear fusion, the stellar envelope

expands and cools down. After an iron core is formed, fusion stops due to iron's highest binding energy per nucleon and the temperature doesn't rise anymore. The core of the star with iron group elements has a mass $\simeq 1.4 M_{\odot}$ and diameter $\sim 6 \times 10^3\ km$ (similar to a white dwarf density) which collapses to the scale of a neutron star [14] (diameter $\sim 30\ km$) within a second due to lack of counter-pressure against its own gravity, causing an explosion that results in a core-collapse supernova (CCSN) [15].

The energy liberated in such a collapse is the same as the increase in the gravitational binding energy of the core (typically $\sim 10^{53}\ erg$) and is easily estimated. It turns out that the kinetic energy of the outgoing stellar envelope released in the explosion is ∼1% of the gravitational binding energy of the core in such a supernova and the energy released in electromagnetic radiation is about ∼1% of the former [16]. The outer envelope of a pre-collapsed star is usually more massive than the core, but also much less dense (diameter $\sim 6 \times 10^8\ km$) and less gravitationally bound due to the small core. So, the energy required to completely destroy the envelope is just a small fraction of the energy released in the core collapse [15].

The CCSNe generally leaves either a neutron star or a black hole [17] depending upon the properties of the core during the collapse with low-mass degenerate cores forming neutron stars, higher-mass degenerate cores mostly collapsing completely to black holes, and non-degenerate cores undergoing runaway fusion [18][19]. The higher-mass degenerate cores that collapse into black holes do not result in a visible supernova [20]. This happens because the core collapse is never stopped by the degeneracy pressure due to its large mass and the mechanism that produces an explosion never happens.

The four images in Fig. 1.4 are snapshots from a 20s animation and show a massive star exploding in a CCSN. As the fusion continues inside the star, eventually it can't support its own weight and the star collapse [21]. These snapshots are described as:

- at t=0s, there is a pre-collapse star generally a red supergiant.

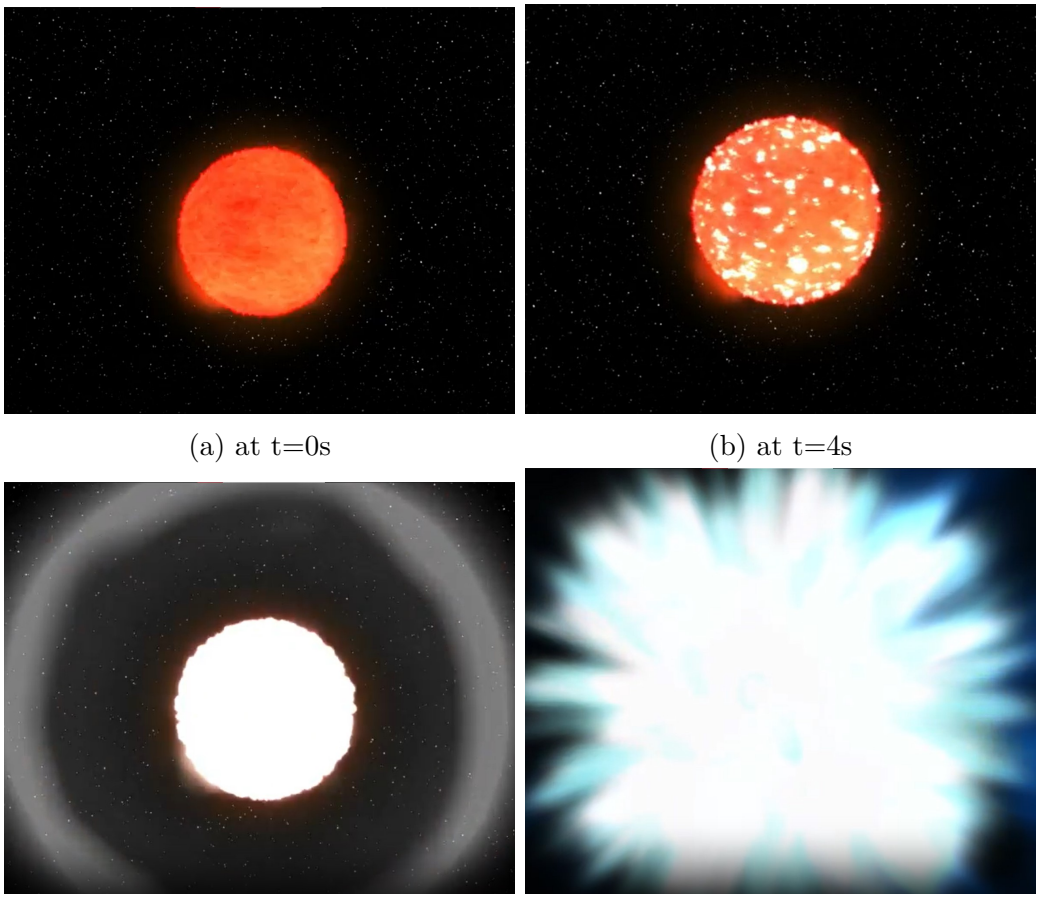

(a) at t=0s (b) at t=4s

(c) at t=8s (d) at t=10s

Figure 1.4: Snaps of a core-collapse supernova(CCSN) from an animation [21] Credits: NASA/JPL-Caltech

- at t=4s, the core is collapsing and the temperature rises.
- at t=8s, a bounce shock expands, driven by the collapse and probably powered by neutrinos produced through photo-disintegration and neutronization inside the core.
- at t=10s, a supernova explosion occurs due to the transfer of a fraction of energy from the core collapse to the stellar envelope.

1.2 Neutrinos

A neutrino is a neutral elementary particle with a spin of 1/2 (also called a fermion) that only interacts via weak interaction and gravity but shows no strong interaction

[22]. The rest mass of the neutrino is very small as compared to other elementary particles excluding gluon and photon whose rest mass is zero [23]. Due to the short range of weak force and weak gravitational interaction of neutrinos, they pass through normal matter unimpeded and undetected [24][25].

There are three flavors of neutrinos created by weak interactions [24], each associated with one of the leptons:

- electron neutrino (ν_e) associated with electrons (e^-),
- muon neutrino (ν_μ) associated with muons (μ^-),
- tau neutrino (ν_τ) associated with tau particles (τ^-)

Initially, neutrinos were thought to be massless but later it was found that there exist three distinct neutrino masses, however, each flavor state of neutrino is a specific superposition of all the three mass states and the exact mass values are unknown as of now. There also exists a unique phenomenon with neutrinos called oscillation in which a definitive flavor of neutrino can be measured to change flavor states while traveling long distances (in kms) [24].

They are also known to have a neutral antiparticle known as anti-neutrinos which differs from corresponding neutrinos by having a lepton number with an opposite sign and a right-handed chirality instead of left-handed.

1.2.1 Neutrino production

Neutrinos are produced in various sources by radioactive decay. Some of these are:

- β-decay of atomic nuclei or hadrons,

  The study of beta decay provided the first physical evidence for the existence of the neutrino due to the non-conservation of energy and angular momentum in the reaction.

β^- *decay* : $n \rightarrow p + e^- + \bar{\nu}_e$ β^+ *decay* : $p \rightarrow n + e^+ + \nu_e$

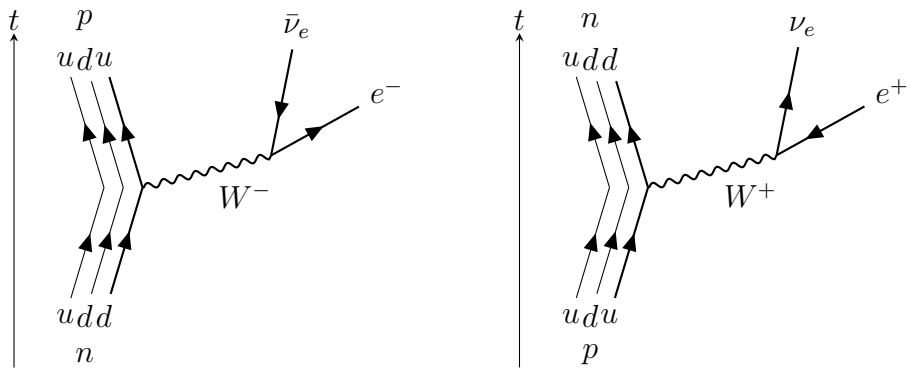

The Feynman diagram on the left is associated with β^- decay whereas the right is for β^+ decay.

These Feynman diagrams show the fundamental process of neutrino production where an up(down) quark changes to a down(up) quark by emitting a W^+/W^- boson respectively that later decays into a pair of fermions, constituting neutrino and positron or anti-neutrino and electron keeping lepton number preserved.

- nuclear reactions like in the core of a star, nuclear reactors, nuclear bombs, or particle accelerators

  These reactions have nuclear fusion and fission chain reactions going on till the particles end up or become stable enough to not participate in the reaction.

  Some of the reactions that happen inside a star like our Sun is the $proton - proton$ or $electron - capture$ chain reaction as shown in Fig 1.5.

- during a supernova

  Stars end their life as supernovae with different mechanisms as described in sub-sections 1.1.2 and 1.1.3.

  Though there are neutrinos and antineutrinos coming from SN-Ia (runaway thermonuclear) explosion due to decays of the fusion products that

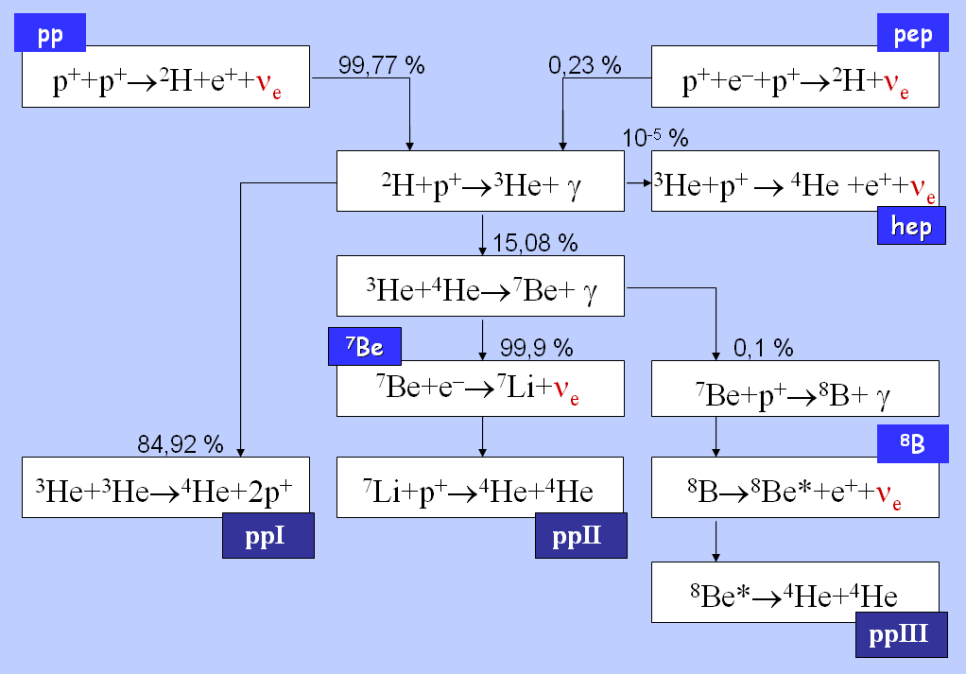

Figure 1.5: Different reactions taking place inside the star's core producing neutrinos Credits: Wikipedia

are beta unstable, most of the energy is released as the kinetic energy of the ejecta and electromagnetic radiation, which is driven by the decays of the iron group elements.

In core-collapse supernovae, most of the energy is directed into neutrino emission, and some of this apparently powers the observed destruction as described in 1.1.3. 99%+ of the neutrinos escape the star in the first few minutes following the start of the collapse. High-energy(non-thermal) neutrinos also originate when the particles accelerate at the forward shock from collapse in the stellar envelope, or when the SN ejecta interacts with the circumstellar medium (CSM) around the star, about which we will talk in Chapter 2.

- when cosmic rays or accelerated particle beams strike atoms

  Cosmic rays are high-energy particles primarily consisting of protons or atomic nuclei that move through space at nearly the speed of light. They have different sources of origin which can be some star or a distant galaxy.

When a cosmic ray from space interacts with atoms in Earth's atmosphere it produces a shower of particles like pions(π), kaons(K), and heavy baryons which are unstable and further decay into photons(γ), and leptons($e,\ \mu,\ \nu_{e/\mu}$) which include neutrinos.

Some of the reactions that take place in the air shower before we observe photons, muons, electrons, and neutrinos at the ground are :

$\pi^0 \rightarrow \gamma + \gamma$ (opposite spin photons); $\pi^+ \rightarrow \mu^+ + \nu_\mu$ (similarly for π^-); $K^\pm \rightarrow \pi^\pm + \pi^0$; $K^+ \rightarrow \mu^+ + \nu_\mu$ (similarly for K^-, there might be different decay channels for a particle); $\gamma \rightarrow e^+ + e^-$; $\mu^+ \rightarrow e^+\nu_e + \bar{\nu}_\mu$ (similarly for μ^-) [26].

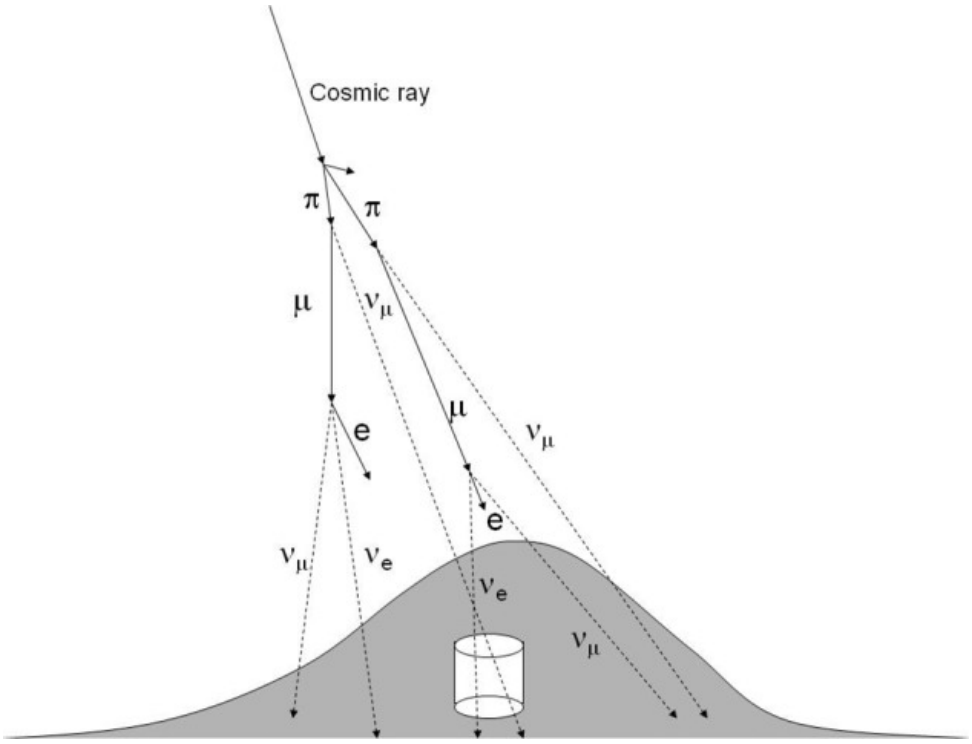

Figure 1.6: Production of neutrinos by cosmic-ray interactions with atoms in the Earth's atmosphere. It happens around 15km above the ground [27].

1.2.2 Neutrino Astronomy

Neutrino astronomy is the branch of astronomy that observes astronomical objects with the help of neutrinos. When astronomical bodies are studied using light, only

the surface of the object can be directly observed. Any photons produced in the core of a star will interact with particles in the outer layers of the star, taking thousands of years to reach the surface. Neutrinos rarely interact with matter, unlike photons. Therefore, neutrinos offer a special method to observe what's happening inside astronomical objects with high matter density that restrict photons to emerge instantly and hence, hidden from optical telescopes, such as reactions in the Sun's core.

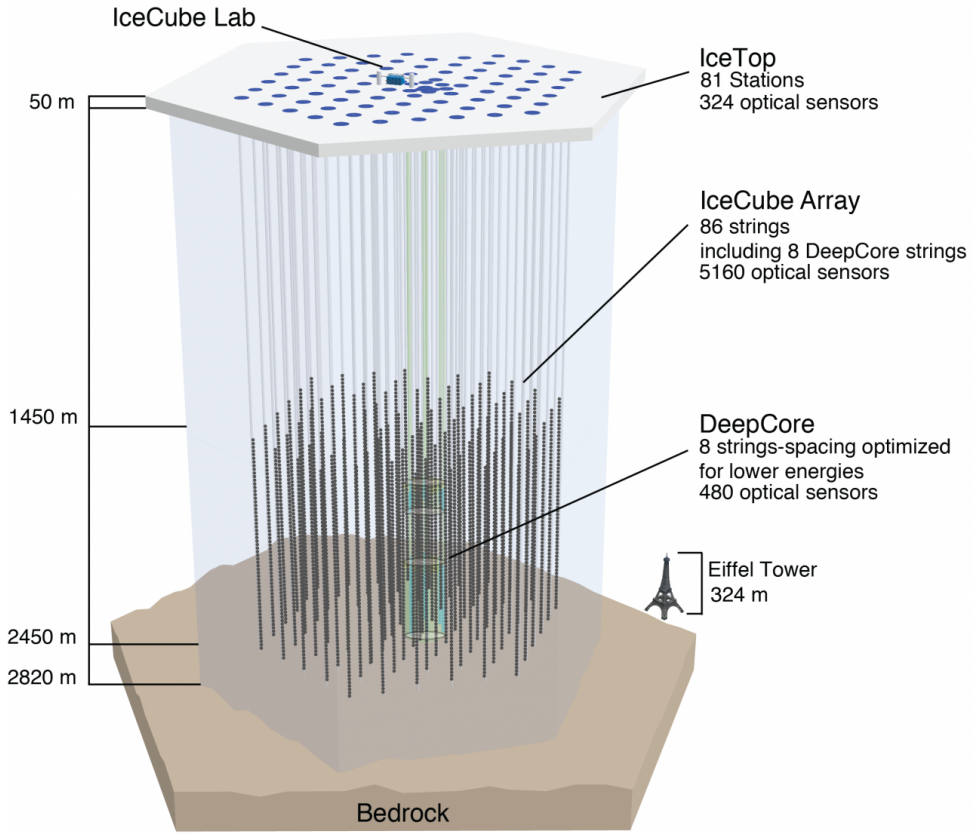

Figure 1.7: IceCube Neutrino Observatory with the in-ice array, sub-array DeepCore, and the cosmic-ray air shower array IceTop [28].

Since neutrinos interact weakly, neutrino detectors have large target masses, thousands of tons. Currently, there are many functioning neutrino observatories all around the globe like IceCube, Hyper-Kamiokande (Hyper-K), Jiangmen Underground Neutrino Observatory (JUNO), India-based Neutrino Observatory (INO), Baikal Deep Underwater Neutrino Telescope, Cubic Kilometre Neutrino Telescope (KM3NeT), Neutrino Ettore Majorana Observatory (NEMO), etc.

Some of the applications of neutrino astronomy are -

- Supernova alert system - Seven neutrino experiments: Super-K, LVD, IceCube, KamLAND, Borexino, Daya Bay, and HALO work together as the Supernova Early Warning System (SNEWS) [snews.bnl.gov].

  In a core collapse, while photons are trapped for hours, neutrinos escape in seconds and most of the energy is released in neutrinos. So, they can reach Earth before photons do. If more than one SNEWS detectors observe an increased flux of neutrinos coincidentally, an alert is sent to prepare for supernova observation. The alert can also point toward the supernova's location in the sky by using the distance between detectors and the time difference between detections.

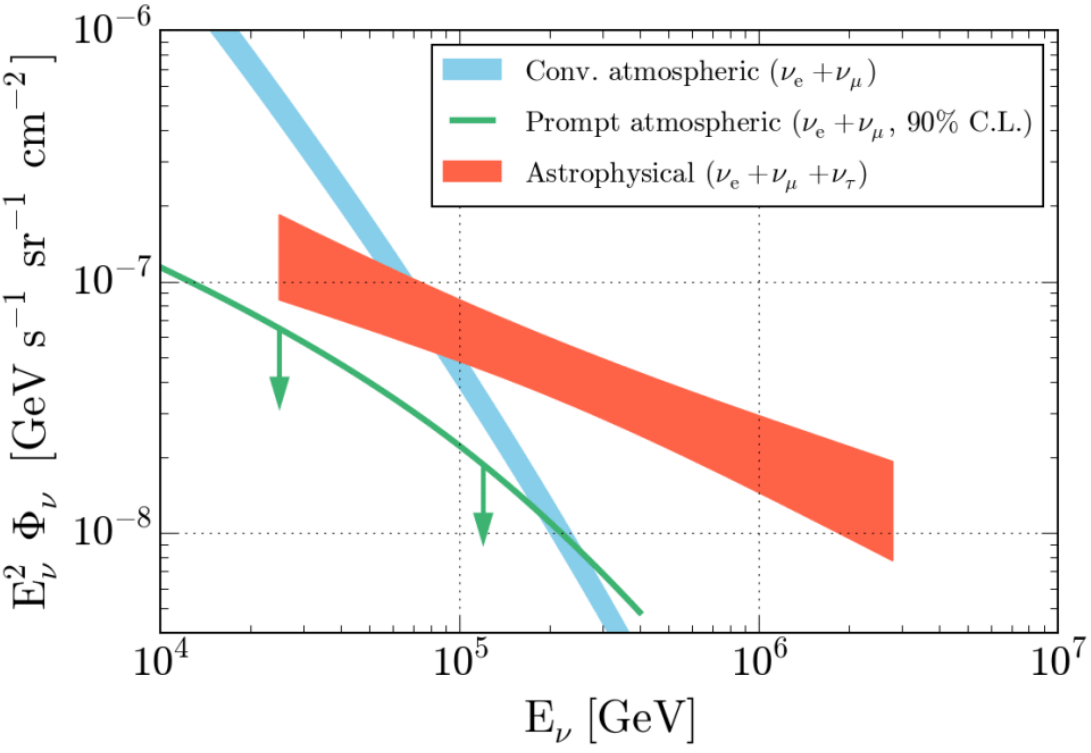

Figure 1.8: Energy spectrum of the astrophysical neutrino flux vs atmospheric neutrino flux from kaon and pion decay(blue shaded) and charmed decay(green line) Credits: IceCube Collaboration

- High-energy astrophysical events - Neutrinos can either be produced in astrophysical processes or from cosmic ray interactions. We have discussed the

latter in 1.2.1. At low energies, the flux of atmospheric neutrinos is greater than astrophysical neutrinos whereas the astrophysical neutrino flux dominates at high energies ($\sim 10^2\ TeV$) as shown in Fig 1.8.

There are many sources of high-energy neutrinos like compact binary pairs of black holes and neutron stars, supernovae, gamma-ray bursts, active galactic nuclei, and relativistic jets. If the neutrino interacts within a detector and produces a muon, the muon will produce an observable track. At high energies, the neutrino direction and muon direction are closely correlated which helps in tracing the source of neutrino [29].

These neutrinos and cosmic rays from different astrophysical processes along with electromagnetic and gravitational observations from different sources can provide better information and are probes of multi-messenger astronomy.

Chapter 2

Theory

This work focuses on high-energy (non-thermal) neutrino production that might be observed from a core-collapse supernova(CCSN) or choked jets in a roughly estimated distance of 10 kpc from Earth which reaches the center of the Milky Way(MW) galaxy.

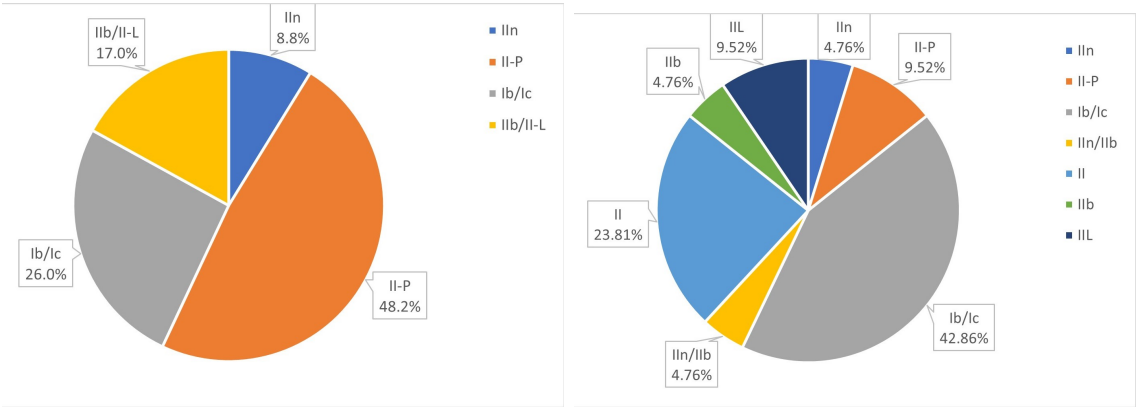

Figure 2.1: (*Left*) Local rate of core-collapse SNe [30]. Type II-P followed by Ib/c are the most common ones at z = 0. (*Right*) Additional distribution of 21 expected SN candidates in Milky Way A.1 suggesting Ib/c as a probable SN type candidate.

The distribution of different CCSN types varies with redshift due to the change in the density of stars and varying metallicity of the host galaxies seen at higher redshift. Unfortunately, the distribution of CCSN types at increasing redshift is uncertain, and limited information is available up to z = 1 [31]. So, to take into

account that some CCSN types are more common than others, we assume that the distribution of CCSN types at z = 0 shown in Fig 2.1 is also true at higher redshift [30].

So, IIP and Ib/c are the most probable CCSN type that may occur in MW and hence, I chose to work on high-energy neutrino production from these two SN types in Milky Way. While IIP candidates produce most of the high-energy neutrinos from the CSM-ejecta interaction, Ib/c is also believed to harbor jets inside which amounts to explain the observed neutrino and photon spectra. I considered different models that lead to high-energy neutrino production from CCSN and jets.

These mechanisms lead to TeV neutrino production through non-thermal particle acceleration like diffusive shock acceleration (Fermi acceleration) and different particle scattering/interaction like proton-proton collision, photo-proton collision, synchrotron, inverse-Compton, and the Bethe-Heitler process decides the cooling timescale of particles which we describe in **??**.

2.1 Models

My theory model mainly includes all the information from references [32][33][34][35][36][37][38][39][40][41][42][43][44] and other references mentioned in these papers.

2.1.1 CSM-ejecta interaction

The circumstellar material is a result of progenitors' mass loss in the past few months to years before the supernova. So, progenitors with different properties are responsible for different SNe, and the neutrino production depends on the CSM properties and SN ejecta kinetic energy. CSM – ejecta interaction happens when supernova ejecta after the explosion propagates in a radially outward direction and starts to interact with the CSM, generating a shock-front moving along with ejecta that accumulates the CSM, which at a later time is also responsible for the deceleration of the shock. IIP has been a promising candidate for this interaction.

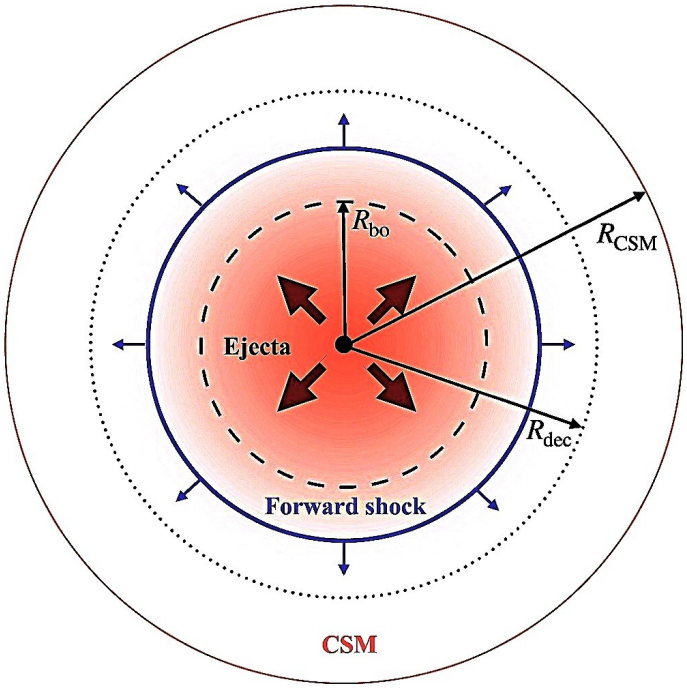

Figure 2.2: Sketch of assumed spherically symmetric SN explosion. The outer edge of the CSM is marked as R_{csm}. The dashed line marks the position of the breakout radius (R_{bo}) whereas the dotted line marks the deceleration radius of the ejecta (R_{dec}). The interaction of the SN ejecta (dark red coloured region) with the CSM leads to the formation of shocks that propagate radially outwards (blue line)[34].

We assume a spherical, steady and wind-like circumstellar medium (CSM) with solar composition ejected from the massive progenitor in the final stages of its evolution. We define its number density profile as-

$$n_{CSM}(R) = \frac{\rho_{CSM}(R)}{m} = \frac{\dot{M}}{4\pi v_w m R^2} \tag{2.1}$$

where $\dot{M}$ is the stellar mass loss rate, v_w the wind velocity, $m = \mu mH$; with μ = 1.3 being the mean molecular weight for a neutral gas of solar abundance, and R the distance to the stellar core.

We assume that spherically symmetric SN ejecta of mass M_{ej} and kinetic energy E_k expand in the surrounding CSM homologously. The CSM extends up to an external radius RCSM. The outer ejecta density profile, which is relevant for the interactions leading to neutrino production, scales as $n_{ej} \propto R^{-s}$, where we assume s = 10. The shocked SN ejecta and CSM form a thin dense shell because of efficient

radiative cooling. Being the thickness of the thin shocked shell much smaller than its radius, one can describe its evolution through the radius $R_{sh}(t)$. In the ejecta-dominated phase, namely in the phase in which most part of the ejecta is still freely expanding (i.e. when the mass of the ejecta is larger than the swept-up CSM mass), the shock radius is given by:

$$R_{sh}(t) = \left[\frac{2}{s(s-4)(s-3)}\frac{v_w}{\dot{M}}\frac{[10(s-5)E_k]^{(s-3)/2}}{[3(s-3)M_{ej}]^{(s-5)/2}}\right] \tag{2.2}$$

with the corresponding shock velocity $v_{sh} = \frac{\mathrm{d}R_{sh}}{\mathrm{d}t}$. But we have kept a constant shock velocity, as it doesn't introduce much difference.

Because of the high CSM density, the forward shock is initially expanding in a radiation-dominated region, and particle acceleration is not efficient. Efficient particle acceleration takes place at radii larger than that of the shock breakout (R_{bo}), where initially trapped photons are free to diffuse out to the photosphere; the shock breakout radius is computed by solving the following equation:

$$\tau_T(R_{bo}) = \int_{R_{bo}}^{R_{csm}} \rho_{CSM}(R)\kappa_{es}dR = \frac{c}{v_{sh}} \tag{2.3}$$

where $\kappa_{es} = 0.34\ cm^2g^{-1}$ is the electron scattering opacity at solar abundances, and c is the speed of light. When the SN ejecta mass M_{ej} becomes comparable to the swept-up mass from the CSM, the ejecta enters the CSM-dominated phase. This transition happens at the deceleration radius. For $R > R_{dec}$, the forward shock radius evolves as given by

$$R_{sh}(t) = R_{dec}\left(\frac{t}{t_{dec}}\right)^{2/3} \quad ; \tag{2.4}$$

where ,

$$R_{dec} = \frac{M_{ej}v_w}{\dot{M}}$$

here, we have assumed adiabatic dynamical evolution for the sake of simplicity. At radii larger than R_{bo}, diffusive shock acceleration of the incoming CSM protons takes

place. The proton injection rate for a wind density profile is

$$Q_p(\gamma_p, R) \equiv \frac{\mathrm{d}^2 N_p}{\mathrm{d}\gamma_p \mathrm{d}R} \simeq \frac{9\pi\epsilon_p R_{bo}^2 n_{bo}}{8 \ln\left[\frac{\gamma_{p,max}}{\gamma_{p,min}}\right]} \left[\frac{v_{sh}(R_{bo})}{c}\right]^2 \left(\frac{R}{R_{bo}}\right)^{2\alpha} \times \gamma_p^{-k} H(\gamma_p - \gamma_{p,min}) H(\gamma_{p,max} - \gamma_p) \quad (2.5)$$

where the parameter α dictates the radial dependence of the shock velocity ($v_{sh} \propto R^\alpha$), it is $\alpha = -1/7$ in the free expansion phase ($R < R_{dec}$) and $\alpha = -1/2$ in the decelerating phase ($R > R_{dec}$). ϵ_p is the fraction of the shocked thermal energy stored in relativistic protons and $H(x)$ is the Heaviside function.

We set the proton spectral index $k = 2$ and the minimum Lorentz factor of the accelerated protons $\gamma_{p,min}$= 1. The maximum Lorentz factor of protons $\gamma_{p,max}$ is obtained by requiring that the acceleration timescale is shorter than the total cooling timescale for protons: $t_{acc} \leq t_{p,cool}$.

$$t_{acc} \sim 20\gamma_p m_p c^3 / 3eBv_{sh}^2; \quad (2.6)$$

$$where, \quad B = \sqrt{32\pi\epsilon_B m_p v_{sh}^2 n_{CSM}} \quad (2.7)$$

B is the magnetic field in the post-shock region, whose energy density is a fraction ϵ_B of the post-shock thermal energy density. The latter is obtained by considering the Rankine-Hugoniot jump conditions across a strong non-relativistic shock with a compression ratio approximately equal to 4.

The most relevant energy loss mechanisms for protons are inelastic pp collisions and the cooling due to adiabatic expansion of the shocked shell, hence,

$$t_{p,cool}^{-1} = t_{pp}^{-1} + t_{ad}^{-1}$$

, where

$$t_{pp} = (4k_{pp}\sigma_{pp}n_{CSM}c)^{-1} \tag{2.8}$$

$$t_{ad} = min[t_{dyn}, t_{cool}] \tag{2.9}$$

$$t_{dyn} = v_{sh}/R_{sh} \tag{2.10}$$

$$t_{cool} = \frac{3k_BT}{2n_{sh}\Lambda(T)} \tag{2.11}$$

we assume constant inelasticity $k_{pp} = 0.5$ and energy-dependent cross-section $\sigma_{pp}(E_p)$. k_B is the Boltzmann constant, $n_{sh} = 4n_{csm}$ is the density of the shocked region, and $\Lambda(T)$ is the cooling function capturing the physics of radiative cooling. Here T is the gas temperature immediately behind the forward shock front obtained by the Rankine-Hugoniot jump conditions, given by:

$$T = 2\frac{(\gamma-1)}{(\gamma+1)^2}\frac{mv_{sh}^2}{k_B}$$

$$\Lambda(T) = \begin{cases} 6.2\times10^{-19}T^{-0.6}, & 10^5K < T \leq 4.7\times10^7K \\ 2.5\times10^{-27}T^{0.5}, & T > 4.7\times10^7K \end{cases}$$

where γ=5/3 is the adiabatic index of the gas and the units of the cooling function $\Lambda(T)$ is given by $erg\ cm^3\ s^{-1}$.

Relativistic protons in the shocked region may also interact with the ambient photons via $p\gamma$ interactions. However, in this work, we ignore this energy loss channel as $p\gamma$ interactions can be safely neglected for a wide range of parameters.

The evolution of the proton distribution is given by:

$$\frac{\partial N_p(\gamma_p,R)}{\partial R} - \frac{\partial}{\partial\gamma_p}\left[\frac{\gamma_p}{R}N_p(\gamma_p,R)\right] + \frac{N_p(\gamma_p,R)}{v_{sh}(R)t_{pp}(R)} = Q_p(\gamma_p,R) \tag{2.12}$$

where $N_p(\gamma_p, R)$ represents the total number of protons in the shell at a given radius R with Lorentz factor between γ_p and $\gamma_p + \mathrm{d}\gamma_p$. The second term on the left side of eq 2.12 takes into account energy losses due to the adiabatic expansion of the SN shell, while pp collisions are treated as an escape term as they do not affect the evolution of

the high-energy cutoff of the distribution but just the number of available protons. Other energy loss channels for protons are negligible. Furthermore, the diffusion term has been neglected since the shell is assumed to be homogeneous.

For a generic source term of protons, $Q_p(\gamma_p, R)$, the proton distribution as a function of shock radius is given by:

$$N_p(\gamma_p, R) = \int_{R_bo}^{R} Q_p(\gamma_0, r_0)\frac{\gamma_0}{\gamma_p} f_p(R, r_0)\mathrm{d}r_0 \tag{2.13}$$

where,

$$\gamma_0 = \gamma\left(\frac{R}{r_0}\right)$$

and

$$f_p(R, r_0) = \exp\left[-\frac{A_{pp}}{q_{pp}}\left(\frac{R_{bo}}{r_0}\right)^{q_{pp}}\left(1 - \left(\frac{r_0}{R}\right)^{q_{pp}}\right)\right]$$

In the above equation, we introduced $q_{pp} = w - 1 + \alpha$ and $A_{pp} = 10(w-1)\beta_{0,-1}^{-2}$.

The neutrino production rates, $Q_{\nu_i+\bar{\nu}_i}[GeV^{-1}cm^{-1}]$, for muon and electron flavor (anti)neutrinos are given by :

$$Q_{\nu_\mu+\bar{\nu}_\mu}(E_\nu, R) = \frac{4n_{CSM}(R)m_pc^3}{v_{sh}}\int_0^1 dx\frac{\sigma_{pp}(E_\nu/x)}{x}N_p(E_\nu/xm_pc^2, R) \\ (F^1_{\nu_\mu}(E_\nu, x) + F^2_{\nu_\mu}(E_\nu, x)) \tag{2.14}$$

$$Q_{\nu_e+\bar{\nu}_e}(E_\nu, R) = \frac{4n_{CSM}(R)m_pc^3}{v_{sh}}\int_0^1 dx\frac{\sigma_{pp}(E_\nu/x)}{x} \\ N_p(E_\nu/xm_pc^2, R)F_{\nu_e}(E_\nu, x) \tag{2.15}$$

where $x = E_\nu/E_p$. The functions $F^1_{\nu_\mu}$, $F^2_{\nu_\mu}$ *and* F_{ν_e} are from **paper**. Equations 2.14 and 2.15 are valid for $E_p > 100$ GeV, corresponding to the energy range under investigation.

2.1.2 Choked jet model

Choked Jets in low-luminosity gamma-ray bursts(LL-GRBs) are a possible explanation for the missing gamma-ray signal as compared to the neutrino signal for which Ib/c is more probable to harbor jets than IIP. The LL-GRBs launched by compact objects like a neutron star or black hole travel for a short duration and stall inside the extended stellar envelope producing neutrinos at the shocks inside.

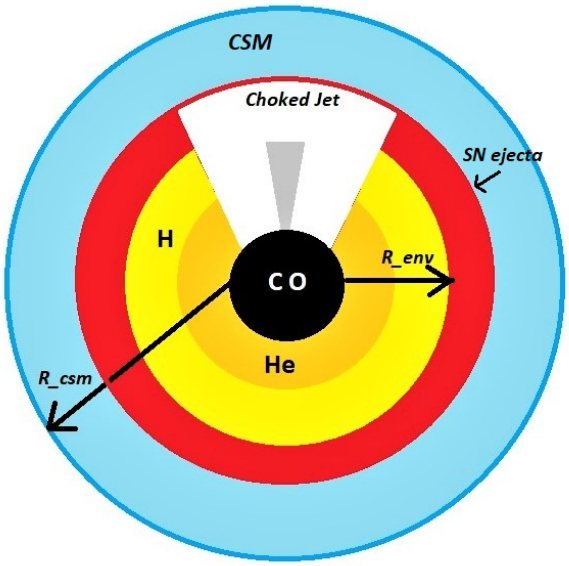

Figure 2.3: The Compact object is surrounded by a helium (He) and hydrogen(H) envelope. The progenitor core is surrounded by an extended stellar envelope of radius R_{env}. The jet(gray) gets choked inside the extended stellar envelope.

We consider a collapsing star that has not lost its H envelope completely, and it is surrounded by an extended shell of radius $R_{env} \simeq 3 \times 10^{13}$ cm and mass $M_{env} \simeq 10^2 M_\odot$. For the extended envelope, we consider the following density profile:

$$\rho_{env} = \rho_{env,0} \left(\frac{R}{R_{env}} \right)^{-2} \tag{2.16}$$

where $\rho_{env,0} = M_{env} \left[\int_{R_{CO}}^{R_{env}} dR 4\pi R^2 \rho_{env}(R) \right]^{-1}$. We assume a fixed-density profile for the extended envelope. The jet is launched near the surface of the CO, with luminosity L_j, and narrow opening angle θ_j.

For fixed θ_j, the dynamics of the jet only depend on the isotropic equivalent

quantities. Hence, it is convenient to define the isotropic equivalent luminosity of the jet: $L_j^{iso} = L_j/(\theta_j/2)^2$. The isotropic equivalent quantities are always defined in the CO frame.

While the jet pierces through the stellar envelope, two shocks develop- a reverse shock propagating back to the core of the jet, and a forward shock propagating into the external envelope. The region between the two shocks constitutes the jet head. Denoting with Γ the Lorentz factor of the unshocked jet plasma (i.e., the bulk Lorentz factor of the jet) and with Γ_h the one of the jet head, the relative Lorentz factor is the following:

$$\Gamma_{rel} = \Gamma\Gamma_h(1 - \beta\beta_h) \tag{2.17}$$

We assume a non-relativistic jet head ($\Gamma_h \simeq 1$), which implies $\Gamma_{rel} \simeq \Gamma$; this assumption is valid for the region of the parameter space of interest.

Here $n'_j = \tilde{L}_j^{iso}/(4\pi R^2 m_p c^3 \Gamma^2)$ is the comoving particle density of the unshocked jet. From the shock jump conditions, we equate the energy densities in the shocked envelope region and in the shocked jet plasma at the position of the jet head $\tilde{R_h} \equiv Rh$, and get the jet head speed for non-relativistic case:

$$e_{sh,env} = (4\Gamma_h + 3)(\Gamma_h - 1)\rho_{env}(R_h)c^2 \tag{2.18}$$

$$e_{sh,j} = (4\Gamma_{rel} + 3)(\Gamma_{rel} - 1)n'_j(R_h)m_p c^2 \tag{2.19}$$

$$v_h \simeq \left[\frac{\tilde{L}_j^{iso}}{(4\Gamma_h + 3)\pi c \rho_{env}(R_h)R_h^2}\right]^{0.5} \tag{2.20}$$

and subsequently $R_h \simeq v_h t/(1+z) = v_h \tilde{t}$, where z is redshift of the source. If $R_h < R_{env}$, the jet is choked inside the stellar envelope.

The jet consists of several shells moving at different velocities. This implies that internal shocks may take place in the jet at $R_{IS} \leq R_h$ when a fast shell catches up and merges with a slow shell. We assume that the internal shocks approach the jet head, i.e., $R_{IS} \simeq R_h$. Efficient particle acceleration at the internal shock takes place only until the shock doesn't become radiative and hence, should follow the condition

given below.

$$n'_p \sigma_T R_{IS}/\Gamma \leq \ min[\Gamma_r^2, 0.1\Gamma_r^3/C] \tag{2.21}$$

where constant $C = 1 + 2\ln\Gamma_r^2$ takes care of pair production, $n'_p \simeq n'_j$ is the proton density of the unshocked jet material and Γ_r is the relative Lorentz factor between the shells in the jet.

Electrons can be accelerated at the reverse shock between the shocked and the unshocked jet plasma. Then, they heat up and rapidly thermalize due to the high Thomson optical depth of the jet head. $n_{e,sh,j} = (4\Gamma_h + 3)n'_j$ is the electron density of shocked jet.

Therefore, the electrons in the jet head lose their energy through thermal radiation, with $e_{sh,j}$ defined above and ϵ_e^{RS} being the fraction of the energy that goes into the electrons. The temperature of the emitted thermal radiation, in the jet head comoving frame, is

$$k_B T_h \simeq \left(\frac{30\hbar^3 c^2 \epsilon_e^{RS} \tilde{L}_j^{iso}}{4\pi^4 R_h^2} \right)^{1/4} \tag{2.22}$$

Thus, the head appears as a blackbody emitting at temperature $k_B T'_{IS} = \Gamma_{rel} k_B T_h$ in the comoving frame of the unshocked jet. The density of thermal photons in the jet head is -

$$n_{\gamma,h} = \frac{19\pi}{(hc)^3}(k_B T_h)^3 \tag{2.23}$$

A fraction $f_{esc} = 1/\tau_{T,h}$ of thermal photons escapes in the internal shock, where their number density is boosted by Γ_{rel}. The resulting energy distribution of thermal photons in the unshocked jet comoving frame is as follows [in units of $GeV^{-1}\ cm^{-3}$]:

$$n'_\gamma(E'_\gamma) \equiv \frac{d^2 N_\gamma}{dE'_\gamma dV'} = A'_{\gamma,j} \frac{E'^{-2}_\gamma}{\exp(E'_\gamma/(k_B T'_{IS})) - 1} \tag{2.24}$$

where, $A'_{\gamma,j} = n'_{\gamma,IS} \left[\int_0^\infty dE'_\gamma n'_\gamma(E'_\gamma)\right]^{-1}$ and $n'_{\gamma,IS} \simeq \Gamma_{rel} f_{esc} n_{\gamma,h}$

Protons are accelerated to a power-law distribution at the internal shock, even though the mechanism responsible for particle acceleration is still under debate. The

injected proton distribution in the jet comoving frame is [in units of $GeV^{-1}\ cm^{-3}$]:

$$n'_p(E'_p) \equiv \frac{d^2N_p}{dE'_p dV'} = A'_p E'^{-k_p}_p \exp\left[-\left(\frac{E'_p}{E'_{p,max}}\right)^{\alpha_p}\right] H(E'_p - E'_{p,min}) \tag{2.25}$$

where $k_p \simeq 2$ is the proton spectral index, $\alpha_p = 1$ simulates an exponential cutoff and H is Heaviside function. $A'_p = \epsilon_p \epsilon_d e'_j \left[\int_{E'_{p,min}}^{E'_{p,max}} dE'_p E'_p n'_p(E'_p)\right]^{-1}$; where ϵ_d is the fraction of the comoving internal energy density of the jet $e'_j = \tilde{L}^{iso}_j/(4\pi R^2_{IS} c\Gamma^2$, which is dissipated at the internal shock, while ϵ_p is the fraction of this energy that goes in accelerated protons.

The minimum energy of accelerated protons is $E'_{p,min} = m_p c^2$, while $E'_{p,max}$ is the maximum energy up to which protons can be accelerated at the internal shock. The magnetic field at internal shock: $B' = \sqrt{8\pi\epsilon_B \epsilon_d e'_j}$. The acceleration timescale of protons for the choked jet case is

$$t'^{-1}_{acc} = \frac{ceB'}{\xi E'_p} \tag{2.26}$$

ξ defines the number of gyroradii needed for accelerating protons, and we assume ξ = 10. Protons accelerated at the shocks undergo several energy loss processes. The total cooling time is

$$t'^{-1}_{p,cool} = t'^{-1}_{ad} + t'^{-1}_{p,sync} + t'^{-1}_{p\gamma} + t'^{-1}_{pp} + t'^{-1}_{p,BH} + t'^{-1}_{p,IC} \tag{2.27}$$

where these quantities (in order mentioned) denote the adiabatic, synchrotron, photo-hadronic ($p\gamma$), hadronic (pp), Bethe–Heitler, and inverse Compton cooling timescales, respectively.

These are defined as follows:

$$t'^{-1}_{ad} = \frac{v}{R} \tag{2.28}$$

$$t'^{-1}_{p,sync} = \frac{4\sigma_T m_e^2 E'_p B'^2}{3m_p^4 c^3 8\pi} \tag{2.29}$$

$$t'^{-1}_{p\gamma} = \frac{c}{2\gamma'^2_p} \int_{E_{th}}^{\infty} dE'_\gamma \frac{n'_\gamma(E'_\gamma)}{E'^2_\gamma} \int_{E_{th}}^{2\gamma'_p E'_\gamma} dE_r E_r \sigma_{p\gamma}(E_r) K_{p\gamma}(E_r) \tag{2.30}$$

$$t'^{-1}_{pp} = cn'_p \sigma_{pp} K_{pp} \tag{2.31}$$

$$t'^{-1}_{p,BH} = \frac{7 m_e \alpha \sigma_T c}{9\sqrt{2}\pi m_p \gamma'^2_p} \int_{\gamma'^{-1}_p}^{E'_{\gamma,max}/m_e c^2} d\epsilon' \frac{n'_\gamma(\epsilon')}{\epsilon'^2} \left((2\gamma'_p \epsilon')^{3/2} \left[\ln(\gamma'_p \epsilon') - \frac{2}{3} \right] + \frac{2^{5/2}}{3} \right) \tag{2.32}$$

$$t'^{-1}_{p,IC} = \frac{3(m_e c^2)^2 \sigma_T c}{16 \gamma'^2_p (\gamma'_p - 1) \beta'_p} \int_{E'_{\gamma,min}}^{E'_{\gamma,max}} \frac{dE'_\gamma}{E'^2_\gamma} F(E'_\gamma, \gamma'_p) n'_\gamma(E'_\gamma) \tag{2.33}$$

where $v = 2c\Gamma$ for the choked jet $\gamma_p = E'_p/m_p c^2,\ \epsilon' = E'_\gamma/m_e c^2,\ E_{th} = 0.150 GeV$ is the energy threshold for photopion production, and $\beta'_p \approx 1$ for relativistic particles. The function $F(E'_\gamma, \gamma'_p)$ follows the definition provided in [**paper**], replacing $m_e \to m_p$. The cross sections for $p\gamma$ and pp interactions, $\sigma_{p\gamma}$ and σ_{pp}, can be found in [**paper**]. The function $K_{p\gamma}(E_r)$ is the $p\gamma$ inelasticity, given by

$$K_{p\gamma}(E_r) = \begin{cases} 0.2 & E_{th} < E_r < 1GeV \\ 0.6 & E_r > 1GeV \end{cases} \tag{2.34}$$

The comoving proton density is $n'_p = \tilde{L}^{iso}_j / (4\pi R^2_{IS} m_p c^3 \Gamma^2)$ for the choked jet. The inelasticity of pp interactions is $K_{pp} = 0.5$.

At the internal shock, the secondary charged mesons undergo energy losses before decaying; in turn, affecting the neutrino spectrum. Protons accelerated at the internal shocks interact with the thermal photons escaping from the jet head and going back to the unshocked jet. Efficient $p\gamma$ interactions take place at the internal shock through Δ^+ channel.

$$p + \gamma \to \Delta^+ \to \begin{cases} n + \pi^+ & 1/3 of all cases \\ p + \pi^0 & 2/3 of all cases \end{cases} \tag{2.35}$$

while we can safely neglect pp interactions at the internal shocks since they are subleading [**results**]. Neutrinos can be copiously produced in the decay chain $\pi^+ \to \mu^+ + \nu_\mu$, followed by the muon decay $\mu^+ \to \bar{\nu}_\mu + \nu_e + e^+$.

We rely on the photohadronic model presented in [**paper**]. Hence, given the injected energy distribution of protons and the distribution of target photons, the

rate of production of secondary particles l (with $l = \pi^{\pm}, K^{+}$) in the comoving frame of the unshocked jet is given by the following [in units of $GeV^{-1}\ cm^{-3}\ s^{-1}$]:

$$Q'_l(E'_l) = c \int_{E'_l}^{\infty} \frac{dE'_p}{E'_p} n'_p(E'_p) \int_{E_{th}/2\gamma'_p}^{\infty} dE'_\gamma n'_\gamma(E'_\gamma) R(x,y) \tag{2.36}$$

where $x = E'_l/E'_p$ is the fraction of proton energy that is given to secondary particles,$y = \gamma'_p E'_l$, and $R(x,y)$ is the response function, which contains the physics of the interaction.

the spectrum at the decay of charged mesons after energy losses as talked above, is

$$Q'^{dec}_l(E'_l) = Q'_l(E'_l) \left[1 - \exp\left(-\frac{t'_{l,cool} m_l}{E'_l \tau'_l}\right)\right] \tag{2.37}$$

where τ'_l is the lifetime of the meson l. The comoving neutrino spectrum from the decayed mesons is as follows [in units of $GeV^{-1} cm^{-3} s^{-1}$]:

$$Q'_{\nu_\alpha}(E'_\nu) = \int_{E'_\nu}^{\infty} \frac{dE'_l}{E'_l} Q'^{dec}_l(E'_l) F_{l\to\nu_\alpha}\left(\frac{E'_\nu}{E'_l}\right) \tag{2.38}$$

where $\alpha = e, \mu$ is the neutrino flavor at production, and $F_{l\to\nu_\alpha}$ is provided in **[paper]**. We do not distinguish between neutrinos and antineutrinos ($\nu_\alpha \equiv \nu_\alpha + \bar{\nu}_\alpha$).

Magnetic fields in the internal shock are not large enough to efficiently cool kaons, which have a larger mass and a shorter lifetime compared to pions and muons. Therefore, they suffer less energy losses and do not contribute significantly to the neutrino spectrum, even though they may become important at high energies.

2.2 Neutrino flux at Earth

On their way to Earth, neutrinos undergo flavor conversion. The observed distribution for the flavor ν_α (with $\alpha = e, \mu, \tau$) is [in units of $GeV^{-1} cm^{-2} s^{-1}$]

$$F_{\nu_\alpha}(E_\nu, z) = \varrho \frac{(1+z)^2}{4\pi d_L^2(z)} \sum_\beta P_{\nu_\beta\to\nu_\alpha}(E_\nu) Q'_{\nu_\beta}(E_\nu \varsigma) \tag{2.39}$$

with $Q'_{\nu_\beta}(E_\nu\varsigma)$ being the neutrino production rate in the comoving jet ($p\gamma$ inter-

actions) or in the center of the explosion (pp interactions) frame, given by Equations 2.38 2.15 and 2.14, respectively. The constant $\varrho = V'_{iso} = 4\pi R_{IS}^3/2\Gamma$ represents the isotropic volume of the interaction region [**paper**] in the choked jet scenario, while $\varrho = v_{sh}$ for CSM–ejecta interaction.

Moreover, the Lorentz conversion factor is $\varsigma = (1+z)/\Gamma$ for the choked jet and $\varrho = (1+z)$ for CSM interaction. The neutrino oscillation probability $P_{\nu_\beta \to \nu_\alpha} = P_{\bar{\nu}_\beta \to \bar{\nu}_\alpha}$ is given by the following [**paper**]:

$$P_{\nu_e \to \nu_\mu} = P_{\nu_\mu \to \nu_e} = P_{\nu_e \to \nu_\tau} = \sin^2 2\theta_{12}/4 \tag{2.40}$$

$$P_{\nu_\mu \to \nu_\mu} = P_{\nu_\mu \to \nu_\tau} = (4 - \sin^2 \theta_{12})/8 \tag{2.41}$$

$$P_{\nu_e \to \nu_e} = (2 - \sin^2 2\theta_{12})/2 \tag{2.42}$$

$\theta_{12} \simeq 33.5 deg$[**paper**]

The neutrino fluence at Earth is :

$$\Phi_{\nu_\alpha}(E_\nu) = \int_{t_i}^{t_f} dt F_{\nu_\alpha}(E_\nu, t) \tag{2.43}$$

for choked-jet scenario, the integral in above equation is replaced by the product with the jet lifetime t_j :

$$\Phi_{\nu_\alpha}(E_\nu) = t_j F_{\nu_\alpha}(E_\nu, t) \tag{2.44}$$

Given the muon neutrino fluence up to the time $t, \Phi_{\nu_\alpha}(E_\nu, t)$, the cumulative number of muon neutrinos expected at IceCube up to the same time is

$$N_{\nu_\alpha}(t) = \int_{E_{\nu,min}}^{E_{\nu,max}} dE_\nu dt F_{\nu_\alpha}(E_\nu, t) A_{eff}(E_\nu, \delta) \tag{2.45}$$

where $E_{\nu,min} = 100 GeV$ and $E_{\nu,max} = 10^8 GeV$ are the minimum and maximum neutrino energies, respectively, and $A_{eff}(E_\nu, \delta)$ is the effective detector area as a function of energy and for a fixed source declination, δ.

Chapter 3

Results

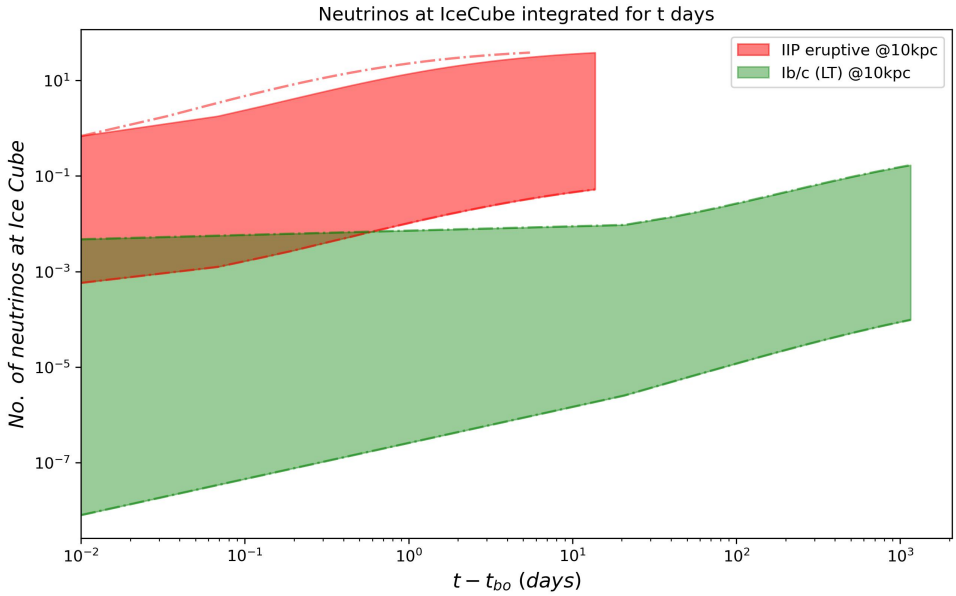

Figure 3.1: Cumulative neutrino flux for IIP and Ib/c csm-ejecta interaction

The parameters are taken from [**paper**]

- parameters for lower limit on SN Ib/c uncertainties
  $\dot{M}_w = 2e-2 * M_\odot/yr, v_w = 1e2 * km/s, r_{out} = 1e17 * cm,$
  $v_s h = 5e3 * km/s, r_{bo} = 5e16 * cm, \epsilon_p = 1e-2, \epsilon_B = 1e-2$

- parameters for upper limit on Ib/c uncertainties
  $\dot{M}_w = 2e-2 * M_\odot/yr, v_w = 1e2 * km/s, r_{out} = 1e17 * cm,$
  $v_s h = 2e4 * km/s, r_{bo} = 5e16 * cm, \epsilon_p = 1e-1, \epsilon_B = 3e-2$

- parameters for lower limit on IIP

  $\dot{M}_w = 1e-2 * M_\odot/yr, v_w = 1e2 * km/s, r_{out} = 1e15 * cm,$

  $v_s h = 8e3 * km/s, r_{bo} = 5e13 * cm, \epsilon_p = 1e-2, \epsilon_B = 1e-3$

- parameters for upper limit on IIP

  $\dot{M}_w = 1e-2 * M_\odot/yr, v_w = 1e2 * km/s, r_{out} = 1e15 * cm,$

  $v_s h = 2e4 * km/s, r_{bo} = 5e13 * cm, \epsilon_p = 1e-1, \epsilon_B = 3e-2$

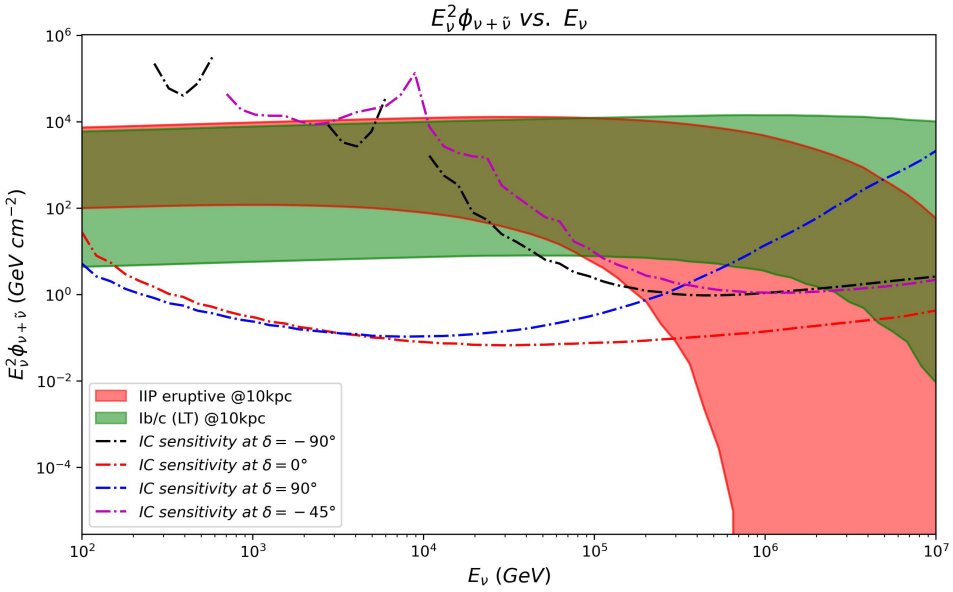

Figure 3.2: Neutrino spectrum for IIP and Ib/c csm-ejecta interaction with IceCube sensitivity

- Parameters for Ib/c choked jet are

  $\theta_j = 0.2, \bar{L}_j = 1e47 * erg/s, \bar{t}_j = 100 * s,$

  $\Gamma = 100, \epsilon_d = 0.2, \epsilon_p = 0.1, \epsilon_B = 0.1, \epsilon_{RS,e} = 0.1$

In figure 3.4 and figure 3.3 we can see its easy detectability by the IceCube detector and the characteristic shape of mesons particle spectra that produced after $p\gamma$ interactions.

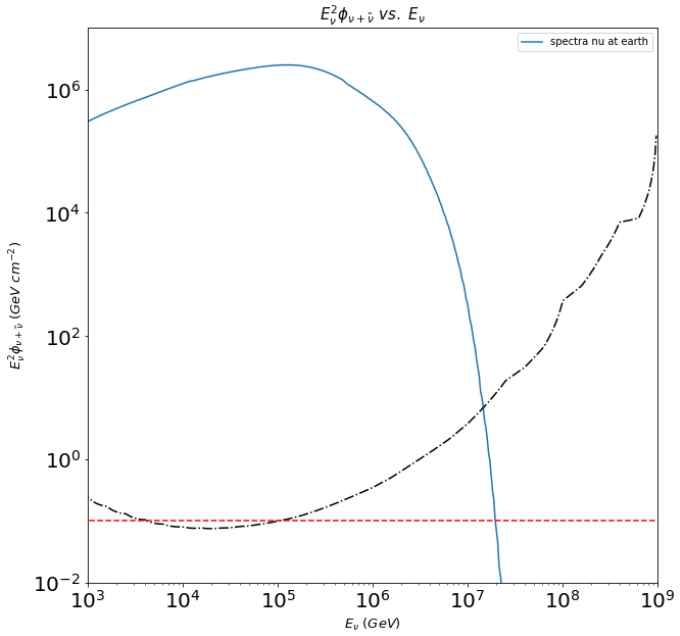

Figure 3.3: neutrino spectra from a typical Ib/c choked jets at 10kpc

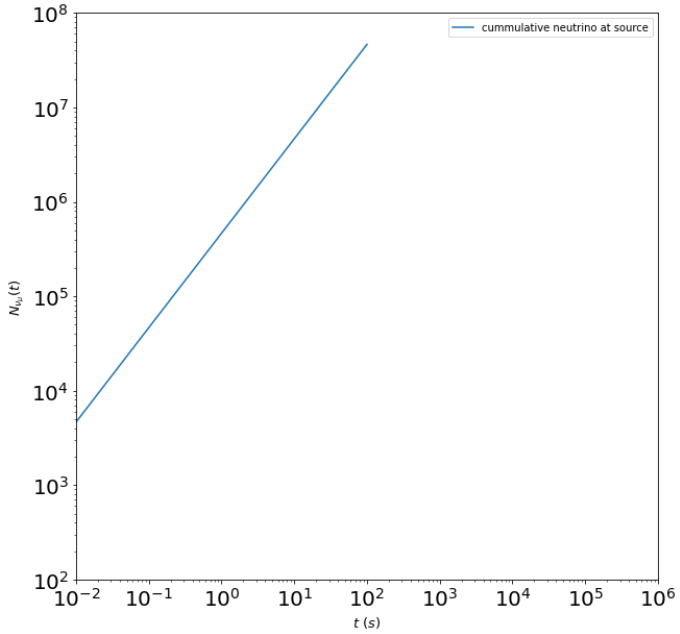

Figure 3.4: cummulative neutrino from a typical Ib/c choked jets at 10kpc

In figure 3.5 shows us that the $p\gamma$ interactions dominate in choked jet scenario.

In figure3.6 Kaons cooling at higher energies than proton energy indicates its no

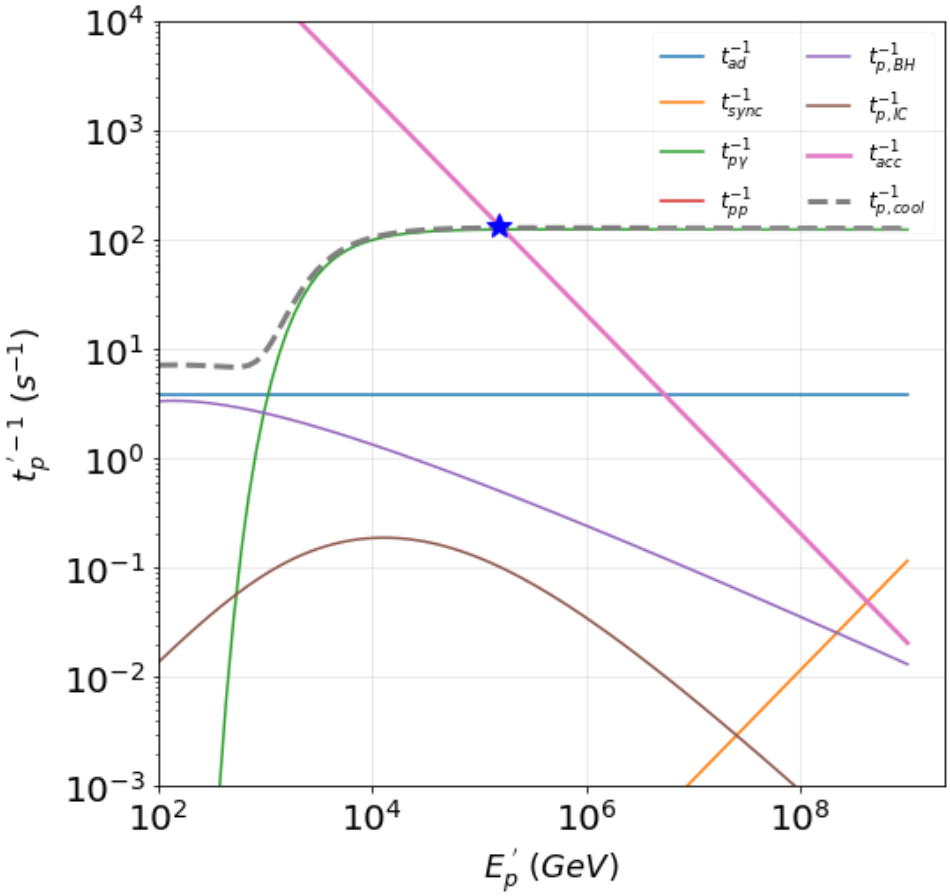

Figure 3.5: Cooling timescales of protons

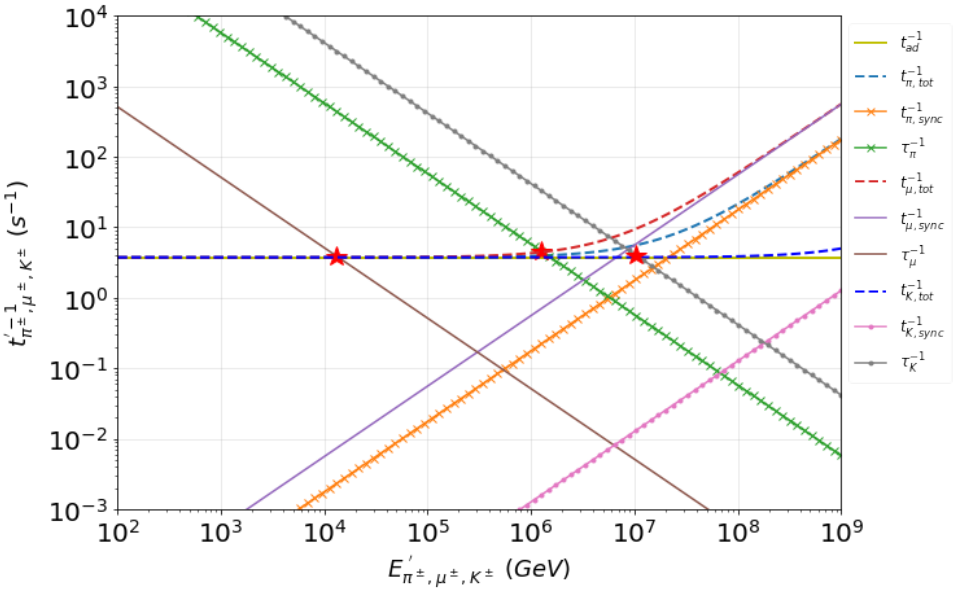

Figure 3.6: Cooling timescales of charged mesons

contribution in the neutrino spectra.

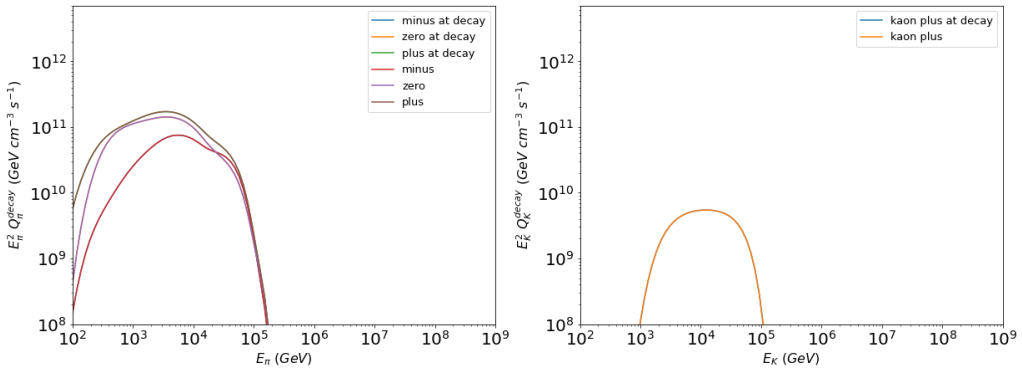

Figure 3.7: pion and kaon spectra before and after decay

In figure 3.7 the difference is not visible at the selected scale but the change appears at the location of the exponential cutoff which makes the curve steeper at decay.

3.1 Future works

- Calculate the signals for a given range of parameters to rule out uncertainty.
- different other signals like precursor neutrino signals or signals from collimated shocks can refine our knowledge for future detection prospects.
- considering a non-constant shock velocity will give us more realistic scenarios.
- we still consider a symmetric evolution of shock profile, which we know is not true in real scenarios.
- exploring mechanism powering the jets or more energetic events can lead us to more meaningful information.

References

[1] *Supernova - Wikipedia*. URL: https://en.wikipedia.org/wiki/Supernova.

[2] *DOE Explains...Supernovae | Department of Energy*. URL: https://www.energy.gov/science/doe-explainssupernovae.

[3] Enrico Cappellaro and Massimo Turatto. "Supernova Types and Rates". In: (2001), pp. 199–214. DOI: 10.1007/978-94-015-9723-4{_}16.

[4] Massimo Turatto. "Classification of Supernovae". In: (2003), pp. 21–36. DOI: 10.1007/3-540-45863-8{_}3.

[5] Hannu Karttunen et al. *Fundamental Astronomy*. Springer Berlin Heidelberg, 2017. DOI: 10.1007/978-3-662-53045-0.

[6] Maryam Modjaz, Claudia P. Gutiérrez, and Iair Arcavi. "New regimes in the observation of core-collapse supernovae". In: *Nature Astronomy* 3.8 (Aug. 2019), pp. 717–724. ISSN: 23973366. DOI: 10.1038/s41550-019-0856-2.

[7] A. Nyholm et al. "Type IIn supernova light-curve properties measured from an untargeted survey sample". In: *Astronomy and Astrophysics* 637 (May 2020). ISSN: 14320746. DOI: 10.1051/0004-6361/201936097.

[8] Anthony L. Piro, Todd A. Thompson, and Christopher S. Kochanek. "Reconciling 56Ni production in type Ia supernovae with double degenerate scenarios". In: *Monthly Notices of the Royal Astronomical Society* 438.4 (2014), pp. 3456–3464. ISSN: 13652966. DOI: 10.1093/mnras/stt2451.

[9] Wen-Cong Chen and Xiang-Dong Li. "On the progenitors of super-Chandrasekhar mass type Ia supernovae". In: (June 2009). DOI: 10.1088/0004-637X/702/1/686. URL: http://arxiv.org/abs/0907.0057%20http://dx.doi.org/10.1088/0004-637X/702/1/686.

[10] D. Andrew Howell et al. "Predicted and observed evolution in the mean properties of Type Ia supernovae with redshift". In: (Jan. 2007). DOI: 10.1086/522030. URL: http://arxiv.org/abs/astro-ph/0701912%20http://dx.doi.org/10.1086/522030.

[11] D. Andrew Howell et al. "The type Ia supernova SNLS-03D3bb from a super-Chandrasekhar-mass white dwarf star". In: *Nature* 443.7109 (Sept. 2006), pp. 308–311. ISSN: 14764687. DOI: 10.1038/nature05103.

[12] M. Fink et al. "Thermonuclear explosions of rapidly differentially rotating white dwarfs: Candidates for superluminous Type Ia supernovae?" In: *Astronomy and Astrophysics* 618 (Oct. 2018). ISSN: 14320746. DOI: 10.1051/0004-6361/201833475.

[13] *Type Ia supernovae: Inside the universe's biggest blasts*. URL: https://www.astronomy.com/science/type-ia-supernovae-inside-the-universes-biggest-blasts/.

[14] S. Woosley and H. -T. Janka. "The Physics of Core-Collapse Supernovae". In: *Nature Physics* 1.3 (Jan. 2006), pp. 147–154. DOI: 10.1038/nphys172. URL: http://arxiv.org/abs/astro-ph/0601261%20http://dx.doi.org/10.1038/nphys172.

[15] Maurizio Spurio. *Probes of Multimessenger Astrophysics Charged Cosmic Rays, Neutrinos, γ-Rays and Gravitational Waves Second Edition Astronomy and Astrophysics Library*. 2nd ed. Springer, 2018. URL: http://www.springer.com/series/848.

[16] H. Th Janka. "Astronomy: The secrets behind supernovae". In: *Science* 297.5584 (Aug. 2002), pp. 1134–1135. ISSN: 00368075. DOI: 10.1126/SCIENCE.1075935/

ASSET/81D4E6AE-7ABD-4639-8E3B-47D12962F3CE/ASSETS/SCIENCE.1075935.FP.PNG. URL: https://www.science.org/doi/10.1126/science.1075935.

[17] A. Heger et al. "How Massive Single Stars End Their Life". In: *The Astrophysical Journal* 591.1 (July 2003), pp. 288–300. ISSN: 0004-637X. DOI: 10.1086/375341.

[18] Jarrod R. Hurley, Onno R. Pols, and Christopher A. Tout. "Comprehensive analytic formulae for stellar evolution as a function of mass and metallicity". In: *Monthly Notices of the Royal Astronomical Society* 315.3 (July 2000), pp. 543–569. ISSN: 00358711. DOI: 10.1046/j.1365-8711.2000.03426.x.

[19] H. Th Janka et al. "Theory of core-collapse supernovae". In: *Physics Reports* 442.1-6 (Apr. 2007), pp. 38–74. ISSN: 03701573. DOI: 10.1016/j.physrep.2007.02.002.

[20] M. Renzo et al. "Predictions for the hydrogen-free ejecta of pulsational pair-instability supernovae". In: *Astronomy and Astrophysics* 640 (Aug. 2020). ISSN: 14320746. DOI: 10.1051/0004-6361/202037710.

[21] *Core collapse supernova – Exoplanet Exploration: Planets Beyond our Solar System*. URL: https://exoplanets.nasa.gov/resources/2174/core-collapse-supernova/.

[22] Dennis Overbye. *Why the Big Bang Produced Something Rather Than Nothing - The New York Times*. 2020. URL: https://www.nytimes.com/2020/04/15/science/physics-neutrino-antimatter-ichikawa-t2k.html.

[23] Susanne Mertens. "Direct Neutrino Mass Experiments". In: *Journal of Physics: Conference Series* 718.2 (June 2016). ISSN: 17426596. DOI: 10.1088/1742-6596/718/2/022013.

[24] Frank Close. *Neutrino (softcover ed.)* Oxford University Press, 2010. ISBN: 9780199695997. URL: https://global.oup.com/academic/product/neutrino-9780199695997?lang=en&cc=us.

[25] Ray Jayawardhana. *The neutrino hunters : The Chase for the Ghost Particle and the Secrets of the Universe*. Oneworld Publications, Jan. 2015. ISBN: 9781780746470. URL: https://oneworld-publications.com/work/the-neutrino-hunters-2/.

[26] M V S Rao and B V Sreekantan. *Extensive Air Showers*. WORLD SCIENTIFIC, Oct. 1998. DOI: 10.1142/3307.

[27] Takaaki Kajita. "Atmospheric neutrinos and discovery of neutrino oscillations". In: *Proceedings of the Japan Academy. Series B, Physical and Biological Sciences* 86.4 (Apr. 2010), p. 303. ISSN: 03862208. DOI: 10.2183/PJAB.86.303. URL: /pmc/articles/PMC3417797/%20/pmc/articles/PMC3417797/?report=abstract%20https://www.ncbi.nlm.nih.gov/pmc/articles/PMC3417797/.

[28] IceCube Collaboration et al. "The IceCube Neutrino Observatory: Instrumentation and Online Systems". In: *Journal of Instrumentation* 12.3 (Dec. 2016). DOI: 10.1088/1748-0221/12/03/P03012. URL: http://arxiv.org/abs/1612.05093%20http://dx.doi.org/10.1088/1748-0221/12/03/P03012.

[29] M. G. Aartsen et al. "Observation of high-energy astrophysical neutrinos in three years of icecube data". In: *Physical Review Letters* 113.10 (Sept. 2014), p. 101101. ISSN: 10797114. DOI: 10.1103/PHYSREVLETT.113.101101/FIGURES/5/MEDIUM. URL: https://journals.aps.org/prl/abstract/10.1103/PhysRevLett.113.101101.

[30] Nathan Smith et al. "Observed fractions of core-collapse supernova types and initial masses of their single and binary progenitor stars". In: *Monthly Notices of the Royal Astronomical Society* 412.3 (2011), pp. 1522–1538. ISSN: 13652966. DOI: 10.1111/j.1365-2966.2011.17229.x.

[31] E. Cappellaro et al. "Supernova rates from the SUDARE VST-Omegacam search. I". In: *Astronomy and Astrophysics* 584 (Sept. 2015). DOI: 10.1051/0004-6361/201526712. URL: http://arxiv.org/abs/1509.04496%20http://dx.doi.org/10.1051/0004-6361/201526712.

[32] S. R. Kelner and F. A. Aharonian. “Energy spectra of gamma-rays, electrons and neutrinos produced at interactions of relativistic protons with low energy radiation”. In: (Mar. 2008). DOI: 10.1103/PhysRevD.78.034013. URL: http://arxiv.org/abs/0803.0688.

[33] Ersilia Guarini, Irene Tamborra, and Raffaella Margutti. “Neutrino Emission from Luminous Fast Blue Optical Transients”. In: (May 2022). DOI: 10.3847/1538-4357/ac7fa0. URL: http://arxiv.org/abs/2205.12282.

[34] Tetyana Pitik et al. “Is the high-energy neutrino event IceCube-200530A associated with a hydrogen-rich superluminous supernova?” In: (Oct. 2021). DOI: 10.3847/1538-4357/ac5ab1. URL: http://arxiv.org/abs/2110.06944.

[35] Soebur Razzaque et al. *HIGH ENERGY NEUTRINOS FROM A SLOW JET MODEL OF CORE COLLAPSE SUPERNOVAE*. Tech. rep. 2018.

[36] Paolo Lipari, Maurizio Lusignoli, and Davide Meloni. “Flavor Composition and Energy Spectrum of Astrophysical Neutrinos”. In: (Apr. 2007). DOI: 10.1103/PhysRevD.75.123005. URL: http://arxiv.org/abs/0704.0718.

[37] P. Mészros. “Gamma-ray bursts”. In: *Reports on Progress in Physics* 69.8 (Aug. 2006), pp. 2259–2321. ISSN: 00344885. DOI: 10.1088/0034-4885/69/8/R01.

[38] Kohta Murase et al. *HIGH ENERGY NEUTRINOS AND COSMIC-RAYS FROM LOW-LUMINOSITY GAMMA-RAY BURSTS?* Tech. rep. 2006.

[39] M. Petropoulou, A. Kamble, and L. Sironi. “Radio synchrotron emission from secondary electrons in interaction-powered supernovae”. In: *Monthly Notices of the Royal Astronomical Society* 460.1 (July 2016), pp. 44–66. ISSN: 13652966. DOI: 10.1093/mnras/stw920.

[40] Weaver T. A. “The structure of supernova shock waves”. In: *ApJS* 32 (Oct. 1976), p. 233. ISSN: 0067-0049. DOI: 10.1086/190398.

[41] Rikard Enberg, Mary Hall Reno, and Ina Sarcevic. “High energy neutrinos from charm in astrophysical sources”. In: *Physical Review D - Particles, Fields, Gravitation and Cosmology* 79.5 (Mar. 2009). ISSN: 15507998. DOI: 10.1103/PhysRevD.79.053006.

[42] Irene Tamborra, Shin'Ichiro Ando, and Kohta Murase. "Star-forming galaxies as the origin of diffuse high-energy backgrounds: Gamma-ray and neutrino connections, and implications for starburst history". In: *JCAP* 2014.9 (Sept. 2014), p. 043. ISSN: 14757516. DOI: 10.1088/1475-7516/2014/09/043.

[43] Svenja Hümmer et al. "Simplified models for photohadronic interactions in cosmic accelerators". In: (Feb. 2010). DOI: 10.1088/0004-637X/721/1/630. URL: http://arxiv.org/abs/1002.1310.

[44] Prantik Sarmah et al. "High energy particles from young supernovae: gamma-ray and neutrino connections". In: (Apr. 2022). DOI: 10.1088/1475-7516/2022/08/011,. URL: http://arxiv.org/abs/2204.03663%20http://dx.doi.org/10.1088/1475-7516/2022/08/011,.

Appendix A

Appendix

A.1 Table for SN candidate in Milky Way

Table A.1 is a list of supernova candidates or stars that are suggested to be supernova progenitors. Type II supernova progenitors include stars with at least 10 solar masses that are in the final stages of their evolution. Prominent examples of stars in this mass range include Antares, Spica, Gamma Velorum, Mu Cephei, and members of the Quintuplet Cluster. The list also includes massive Wolf–Rayet stars, which may become Type Ib/Ic supernovae [Wikipedia].

Out of 21, 9 of the supernova candidates are of type Ib/c, and the rest belong to SN-II, but many of them are unable to be classified in a particular type of SN-II which limits our information.

Identifier	**Distance(in ly)**	**Possible SN type**
Alpha Lupi	465	II
Antares	554	IIP
Betelgeuse	720	IIP
Rigel	1118	IIn
Gamma^2 Velorum	1120	Ib/Ic
Rho Cassiopeiae	3440	IIL
VY Canis Majoris	3930	II
IRAS 17163-3907	3930	II
HD 168625	5250	II
NML Cygni	5250	II
WR 142	5380	Ib/Ic
IRC +10420	5600	IIb
Mu Cephei	5900	IIn/IIb
WR 93b	7470	Ib/Ic
WR 2	7830	Ib/Ic
WR 102	8610	Ib/Ic
Eta Carinae	8630	Ib/Ic
HD 179821	10500	IIL
WR 104	13400	Ib/Ic
WR 38	19700	Ib/Ic
WR 30a	21900	Ib/Ic

Table A.1: SN candidates in MW.
Source Wikipedia